

Supporting Information

Bock et al. 10.1073/pnas.1613883114

SI Text

Corrections of Isotope Data to Address Fractionation in the Firn Caused by Diffusion. Air in firn is subject to diffusion (140). Accordingly, we applied corrections to our measured ice core isotope data as explained in the following two sections.

Correction of $\delta^{13}\text{CH}_4$ and $\delta\text{D}(\text{CH}_4)$ data because of gravitational settling in the firn. Gravitational settling creates a gradient with heavier isotopologues accumulating at the bottom of the diffusive zone. For the heavier isotopes, an enrichment in the range of 0.2–0.5‰ per mass difference is observed in air bubbles of an ice core and can be corrected for using $\delta^{15}\text{N}_2$ measurements (141, 142). Because only the mass difference is decisive, this approach holds for both $\delta^{13}\text{CH}_4$ and $\delta\text{D}(\text{CH}_4)$. For $\delta^{13}\text{CH}_4$, we used interpolated $\delta^{15}\text{N}_2$ records from EDC (51, 136, 143), TALDICE (144), and Vostok (145). Concerning $\delta\text{D}(\text{CH}_4)$, we used the same procedure and datasets for EDC (51, 136, 143). However, for EDML, no complete dataset covering all our samples is available, and we used the mean value (0.44‰) of all EDML $\delta^{15}\text{N}_2$ values given in ref. 146. Note that the glacial/interglacial difference in the last mentioned dataset is only about 0.05‰, and hence, the error introduced because of this simplified approach is much smaller than other measurement uncertainties for $\delta\text{D}(\text{CH}_4)$. All $\delta^{13}\text{CH}_4$ and $\delta\text{D}(\text{CH}_4)$ data presented in the figures of this contribution have been corrected for gravitational settling in the firn.

Correction of $\delta^{13}\text{CH}_4$ data because of diffusive isotopic fractionation in the firn. Isotopologues of a trace gas species (e.g., $\delta^{13}\text{CH}_4$) have a different diffusion constant; hence, if a concentration gradient between the free atmosphere and the bottom of the firn is present, the isotopic signature of the original atmospheric signal changes while it is carried down to the lock-in depth. The phenomenon called diffusive fractionation is described in detail in ref. 129. The authors also provide the mathematical tools to quantify the effect. Using this approach allowed us to calculate the diffusive fractionation correction for our $\delta^{13}\text{CH}_4$ data.

The diffusive column height for each data point was calculated using interpolated $\delta^{15}\text{N}_2$ records from EDC (51, 136, 143), TALDICE (144), and Vostok (145). The CH_4 mixing ratio and its annual changing rate have been determined using a spline approximation [1,000-y cutoff frequency (147)] of the EDC CH_4 data (4). Other than the values given in ref. 129, we further used estimates for the mean annual site temperatures [EDC: -54°C (129), TALDICE: -41°C (148), and Vostok: -55°C (134)] and the mean annual surface air pressure [EDC: 694 mbar (129), TALDICE: 721 mbar (149), and Vostok: 624 mbar (150)] to calculate the diffusion fractionation correction. All new $\delta^{13}\text{CH}_4$ data presented in the figures of this contribution have been corrected for diffusive isotopic fractionation in the firn. The effect for all of our samples is small, because we did not measure $\delta^{13}\text{CH}_4$ samples from time periods with rapidly changing CH_4 mixing ratio. The changes of the measured values are between -0.18% and $+0.08\%$, hence not relevant for any of our conclusions.

The effect is of the same size for $\delta\text{D}(\text{CH}_4)$. Because the uncertainties of this parameter are larger, we choose not to correct our $\delta\text{D}(\text{CH}_4)$ data for diffusive isotopic fractionation in the firn.

Definition of Time Slices for “Typical” Glacial and Interglacial Levels.

We defined time slices that are intended to represent “typical levels” within our isotope records. These time slices are used to quantitatively describe glacial/interglacial amplitudes of $[\text{CH}_4]$, $\delta^{13}\text{CH}_4$, and $\delta\text{D}(\text{CH}_4)$ and assess the shift of both isotopes for the Holocene and the LGM compared with earlier interglacials

and glacials, respectively. The time interval definition in Fig. S1 uses data for glacial maxima characterized by CO_2 concentrations below 210 ppm and CH_4 concentrations below 420 ppb (4, 110). Similarly, data used for interglacial periods have CO_2 concentrations above 260 ppm and CH_4 concentrations above 500 ppb (4, 110). The time periods used are illustrated in Fig. S1, where red and blue shading highlights data for interglacial and glacial time slices, respectively. In Table S1, we summarize $[\text{CH}_4]$, isotope mean and median values of the used time slices.

Note that the intention of this definition is only a simplified first-order view of the presented records, whereas our data show variations within the chosen time slices rather than stable levels. Note that the time interval with the most ^{13}C -depleted values between 115 and 120 ka BP is not included in the MIS 5.5 typical level, because $[\text{CH}_4]$ is already below typical interglacial levels. This $\delta^{13}\text{CH}_4$ minimum is discussed as a special feature in the text.

Box Model to Constrain the CH_4 Budget. Natural methane sources can be differentiated according to their isotopic signatures. For instance, BB and GEM emit relatively isotopically heavy methane (i.e., enriched in ^{13}C and deuterium compared with the averaged source mix). However, the largest natural source type—microbial emissions largely from wetlands—emits methane with an isotopic fingerprint slightly lower in $\delta^{13}\text{CH}_4$ and $\delta\text{D}(\text{CH}_4)$ than the source mix. In addition, isotopic fractionation by the sinks leads to heavier methane in the atmosphere compared with the emissions.

Box model: Setup. To constrain the (isotopic) CH_4 budget, we used the box model presented in refs. 32 and 36, which consists of four boxes (northern and southern troposphere and stratosphere) with prescribed air mass exchange. This model allows one to assess maximal GEM and increased emissions by BB for the Holocene and the LGM compared with previous interglacials and glacials, respectively. To this end, CH_4 sources (both emission strengths and isotopic source signatures) (Table S2) and relative sink contribution (Table S3) are varied within prescribed ranges in the model (refs. 13, 22, 32, 36, and 63 and references therein). The model is run into steady state, and the equilibrium value of the southern tropospheric box is compared with our data constraints (Table S1) for each of the time slices. If the modeled $[\text{CH}_4]$, $\delta^{13}\text{CH}_4$, and $\delta\text{D}(\text{CH}_4)$ values are compatible within the uncertainty (Table S1) with the data constraint, the emission values are recorded as a possible CH_4 budget solution. For each time slice, 10,000 valid runs have been collected.

Box model: Sources. To be consistent with recent work on the current methane budget (63), we distinguish only three source categories here: GEM, BB, and a microbial source including natural sources, such as wetlands, termites, and naturally occurring ruminants. Isotopic signatures of the sources are based on previous work (refs. 13, 32, and 36 and references therein) and the collection in ref. 63 with some modifications. Table S2 shows the $\delta^{13}\text{CH}_4$ values used for the microbial source, BB, and GEM according to ref. 63 with some modifications (see below) and $\delta\text{D}(\text{CH}_4)$ values (refs. 13 and 22 and references therein).

For the interglacial $\delta^{13}\text{CH}_4$ source signatures of the microbial source, BB emission, and GEM, we used the global value given in ref. 63 with two modifications for the microbial source. (i) The modern microbial source used in ref. 63 includes anthropogenic emissions from ruminants and landfills, which bias the natural isotopic source signature. As we investigated the natural budget in this contribution, we removed the waste CH_4 source (which leads to a heavier source mix signature) and decreased emissions

from ruminants, which at present largely reflect livestock in ref. 63, by $80 \pm 20\%$ (which leads to a lighter source mix signature). In the end, these adjustments essentially canceled each other and led to a global mean microbial source signature that is the same as the recent value given in ref. 63 within the error limits. Accordingly, we used a global mean microbial source signature of $-62.2 \pm 1.0\%$ in our model. (ii) The value given in ref. 63 represents a global average; however, previous work (refs. 32, 35–37, 75, 151, and 152 and references therein) has shown that high-latitude wetland sources are depleted in ^{13}C and deuterium. Because the high-latitude wetland sources are mainly located in the Northern Hemisphere, a difference in the isotopic source signatures of the two hemispheres is observed. To account for this difference, we used the geographically resolved wetland emission estimate in ref. 10 and the published data on the IPD of the methane mixing ratio (9, 79, 89, 132) to assess how much of the total wetland emissions are located in the Northern Hemisphere. Aggregating the distribution in ref. 10 into three categories (tropical south, tropical north, and boreal north) leads to a northern fraction of wetland source emissions of 0.6. However, our model runs are consistent with the IPD constraint (9, 79, 89, 132) only when using a northern fraction of 0.7 for the microbial source. This higher ratio is achieved by shifting $17 \text{ Tg CH}_4 \text{ a}^{-1}$ from the southern tropical to the northern tropical region compared with ref. 10. We stress that this small difference is not in conflict with the estimate in ref. 10, which assessed the present day emissions dominated by the anthropogenic sources. In a next step, we assigned $\delta^{13}\text{CH}_4$ and $\delta\text{D}(\text{CH}_4)$ source signatures for the boreal (high-latitude) source, which are 6 and 50% lower, respectively, than the low-latitude sources (refs. 32, 35–37, 75, 151, and 152 and references therein). Using the global source signature value in ref. 63 (see above), this adjustment led to a Northern Hemisphere microbial source signature of -62.6% and a Southern Hemisphere microbial source signature of -61.4% in $\delta^{13}\text{CH}_4$. For $\delta\text{D}(\text{CH}_4)$, we use -323% for the Northern Hemisphere and -313% for the Southern Hemisphere for the microbial source signature in our model (Table S2). These numbers lead to global source signatures of our microbial source of -62.2 and -320% for $\delta^{13}\text{CH}_4$ and $\delta\text{D}(\text{CH}_4)$ as proposed in refs. 63 and 13, respectively.

As shown in refs. 25 and 34, isotopic signatures of biogenic sources (microbial and BB) may have changed on glacial/interglacial timescales. According to ref. 25, we estimate that about one-half of the glacial/interglacial amplitude of $\delta^{13}\text{CH}_4$ is caused by environmental changes leading to source signature changes, whereas the other one-half is accounted for by source mix changes. Hence, we attributed one-half of the averaged $\delta^{13}\text{CH}_4$ differences of MIS 12 minus MIS 11 and MIS 6 minus MIS 5 (Table S1) to a $\delta^{13}\text{CH}_4$ shift of our microbial and BB source signatures and used these shifted source signatures in our model for glacial time slices. Accordingly, the microbial and the BB $\delta^{13}\text{C}$ source signature ranges for glacial time slices are heavier (higher $\delta^{13}\text{CH}_4$) in our model by 2.6% compared with interglacial runs (Table S2).

The geographic distribution of the emissions (i.e., the fraction that is emitted into the northern model troposphere compared with the Southern Hemisphere) has been adjusted, such that the modeled IPD of $[\text{CH}_4]$ is in line with data constraints for the Holocene and the LGM (9, 79, 89, 132). Our best estimates for both interglacial and glacial model setups are northern emissions fractions of 0.7 for the microbial source, 0.7 for BB, and 0.6 for GEM. Note that no IPD information is available for the oldest four time slices used in this study, because no or no reliable atmospheric CH_4 values are available for the Northern Hemisphere from Greenland ice cores. Hence, we used the same source distribution for older time slices (identical input parameters for the older interglacials, MIS 5.5 and MIS 11.3, as for the

Holocene and identical input parameters for the older glacials, MIS 6 and MIS 12, as for the LGM).

To exclude an overestimation of the emissions into the Northern Hemisphere, we additionally performed sensitivity runs where we assumed no latitudinal difference in the CH_4 emissions (i.e., northern emission fractions of 0.5 for all three source categories). Because an IPD is evident at present and persistent for the last 25,000 y (9, 79, 89, 132), this exercise is considered a minimum conservative endmember for the true hemispheric source distribution. Accordingly, we expect true BB/GEM to be between the results of our best guess model runs and these sensitivity runs. For the sensitivity runs, identical emission values (Table S2) and targets (Table S1) have been used with one exception. The calculation of isotopic source signatures according to the procedure described above yielded slightly higher numbers for the microbial source for both $\delta^{13}\text{CH}_4$ and $\delta\text{D}(\text{CH}_4)$, because $15 \text{ Tg CH}_4 \text{ a}^{-1}$ had to be shifted from the northern tropical to the southern tropical region compared with the distribution given in ref. 10. The changed isotopic signatures of the microbial source for the sensitivity model runs are given in Table S2.

Krypton measurement artifacts and consequences for the CH_4 budget. We stress that our new ice core $\delta^{13}\text{CH}_4$ and $\delta\text{D}(\text{CH}_4)$ measurements presented in this study are free of the krypton (Kr) measurement artifact described in refs. 46–48, which arises if Kr interferences are not excluded during the mass spectrometric (MS) analyses. Previous studies relied on measurements including a Kr effect, which leads to biased $\delta^{13}\text{CH}_4$ values that are higher. Specifically, we note that the assessment in ref. 63 is based on Greenland ice core data for the Late Holocene in ref. 64, which were not corrected for a Kr interference during the measurement. Using the differences of Sapart's (64) $\delta^{13}\text{CH}_4$ values with and without Kr effect for standard air bottles with different $[\text{CH}_4]/\text{Kr}$ ratios given in table 2 of ref. 48, we can roughly assess the bias of the Late Holocene $\delta^{13}\text{CH}_4$ dataset. For this exercise, we assume a mixing ratio around 700 ppb (64). Furthermore, assuming no additional amount dependence of $\delta^{13}\text{CH}_4$ in this dataset (which could amplify or dampen the observation), we calculate an offset of these data of approximately $+1.15\%$. If true, the Late Holocene atmospheric value was lower by this amount. As a consequence, lower $\delta^{13}\text{CH}_4$ constraints lead to lower BB and/or GEM estimates compared with the assessment in ref. 63. Using our observed differences of older time periods (Table S1) to scale emissions based on Fig. 2 leads to a reduction of GEM by roughly $6 \text{ Tg CH}_4 \text{ a}^{-1}$ compared with the value given in ref. 63. Note that the total GEM estimate is also strongly dependent on the assumed BB emissions as discussed in the text.

Box model: Sinks. The atmospheric lifetime of methane has been kept constant at 8 y for all performed runs. This approach is in line with several atmospheric chemistry modeling studies, which show little change in the overall lifetime of methane for different climate periods (40–42, 153). In our revised box model, four sinks are implemented (OH oxidation in the troposphere, methanotrophy in soils, a stratospheric sink, and a Cl sink in the marine boundary layer) with fixed fractionation factors (Table S3) (13, 154–156). Note that these sinks differ greatly in their fractionation factors. Accordingly, although the overall lifetime may have stayed constant over time, a change in the relative fraction of each sink to the total lifetime may have had an impact on the isotopic composition of the atmosphere. Moreover, the effect of such sink contribution effects would have a different impact on $\delta^{13}\text{CH}_4$ and $\delta\text{D}(\text{CH}_4)$. Atmospheric methane removal through the four sink processes in our model is scaled according to ref. 10; however, in our Monte Carlo approach, we allow the relative contributions of each sink to vary within certain limits to account for uncertainties in our understanding of the sink attributions (10). Accordingly, the fractional sink of each sink process (in $\text{Tg CH}_4 \text{ a}^{-1}$) was varied independently by $\pm 15\%$. The sum of all individual sink contributions in each Monte Carlo run was then

scaled to balance the total emission for the lifetime of 8 y required to obtain the targeted CH_4 mixing ratio. The resulting ranges of the relative contribution of each sink are given in Table S3.

Also, the sink contributions are different in both hemispheres. The hemispheric distribution of the model sinks is constant for all runs and summarized in Table S3. The tropospheric and stratospheric sinks are split half and half between the northern and southern boxes. The soil sink and the marine chlorine sink are distributed according to the difference in land and ocean coverage in both hemispheres. We choose a partitioning according to the Global Land Cover Facility with unevenly distributed northern fractions of 0.74 and 0.43 for the soil and marine chlorine sinks, respectively (Table S3) (157, 158).

Box model: Results. Contrary to our previous work (32, 36), we do not present normalized probability density functions (nPDFs) for the box model results. This change is because of the fact that using nPDFs is misleading and suggests a likelihood for emission strengths of different sources, which in fact, is an artifact of the Monte Carlo process. Without additional knowledge, each accepted box model solution in line within the uncertainties with the (isotopic) data constraint is equally likely. For example, the higher numbers of accepted model solutions in ref. 32 for short lifetimes in the glacial do not imply that a shorter lifetime is more realistic. Instead, they reflect only that, in the box model approach, where all parameters are varied independently, it is much easier to achieve low glacial CH_4 concentrations by reducing only one parameter, the lifetime, instead of reducing the emissions of all source types at the same time by the correct amount, while not violating the (isotopic) CH_4 budget. The only valid information that should be drawn from the model results is the field of possible emission strengths for each of the given sources. Accordingly, we can exclude all scenarios that do not fulfill the ice core constraint. In this study, we avoid these pitfalls of nPDFs but go beyond previous Monte Carlo approaches by analyzing the emissions of different source types (Fig. 2 and Fig. S7). For example, Fig. 2 shows the variation of possible GEMs under given BB emissions. Similarly, one can derive information for the microbial source for given numbers of BB and/or GEM as shown in Fig. S7 *A* and *B*. For instance, selecting $25 \text{ Tg CH}_4 \text{ a}^{-1}$ for BB

and $30 \text{ Tg CH}_4 \text{ a}^{-1}$ for GEM during interglacials, the microbial source strength is roughly between 150 and $230 \text{ Tg CH}_4 \text{ a}^{-1}$.

The uncertainty of the isotopic signature of the sources and the fractions of the sinks is intrinsically implemented in the model results, because we allowed the Monte Carlo process to pick values from broad ranges of isotopic source signatures (Fig. S7 *C* and *D* and Table S2) and the sink fractions (Table S3). Fig. S7 *C* and *D* shows that the model favors lower emissions from the microbial source for the Holocene and the LGM compared with older time slices, because the heavier isotope targets are more easily achieved by higher emissions of BB and/or GEM.

Results for the sensitivity analysis on the hemispheric distribution of sources are presented in Fig. S7 *E* and *F*. It is not straightforward to reliably quantify the IPD in the past, but it is clear that, for a minimum (zero) IPD in $[\text{CH}_4]$, our BB and GEM maximum estimates are not significantly higher compared with the standard model runs.

Note that, for emissions from marine clathrates (and generally, submarine GEM), which are part of our GEM model source, our scenarios do not take into account isotopic fractionation during oxidation in the water column. This process leads to heavier (higher) numbers in both isotopes for methane reaching the air/sea interface (27, 29, 31, 36, 39, 54, 159). Assuming heavier fingerprints for clathrate emissions into the atmosphere reduces their share to the global budget. The same is true if a heavier carbon isotopic signature is assumed for some sources of GEM as listed in table 1 of ref. 29.

Supplementary Graphs. An overview of all data presented in this study is shown in Fig. S1, which highlights the time intervals used to determine the targets for the box model runs. We underline that Fig. S1 presents additional Bern $\delta^{13}\text{CH}_4$ data between 25 and 80 ka BP, which are not presented in Fig. 1 and have been partly shown in our technical article on the measurement system (47). Furthermore, we present the data shown in Fig. 1 in enhanced and zoomed versions. First, the interglacial periods are highlighted (Fig. S2) and set into context with a recently published speleothem monsoon proxy record (70). Second, we zoom into three presented time intervals: LGM/Holocene, MIS 6/MIS 5.5, and MIS 12/MIS 11.3 (Figs. S3–S5). Finally, we present a figure comparing previously published data to our records (Fig. S6).

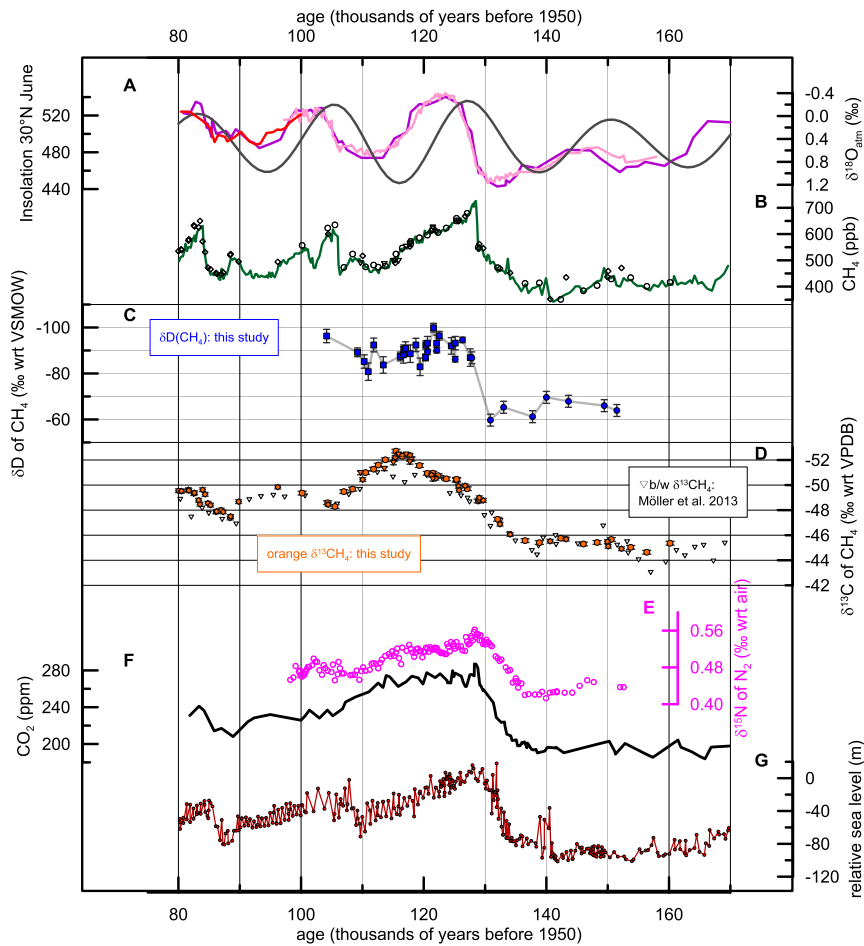


Fig. S4. Paleoclimatic records of Fig. 1 zoomed for MIS 6 and MIS 5.5. From top to bottom, the panels show (A) solar insolation in June at 30° N (133) and atmospheric $\delta^{18}\text{O}$ from Vostok (purple) (134), EDC (light pink) (51, 135–138), and Siple Dome (red) (84); (B) $[\text{CH}_4]$ (ref. 4 and data from this study); (C) $\delta\text{D}(\text{CH}_4)$ from EDML and EDC (this study; error bars are 1-sigma SDs of reference air measurements); (D) $\delta^{13}\text{CH}_4$ from Talos Dome, EDC, and Vostok (5G; this study; the error bars represent the 1-sigma SD of ice core replicates (47): 0.15‰) and data from EDML and Vostok (25, 32). The graph is extended by E showing $\delta^{15}\text{N}$ of air (51). Panel (F) shows $[\text{CO}_2]$ (110); and (G) relative sea level as reconstructed from Red Sea sediment cores (108).

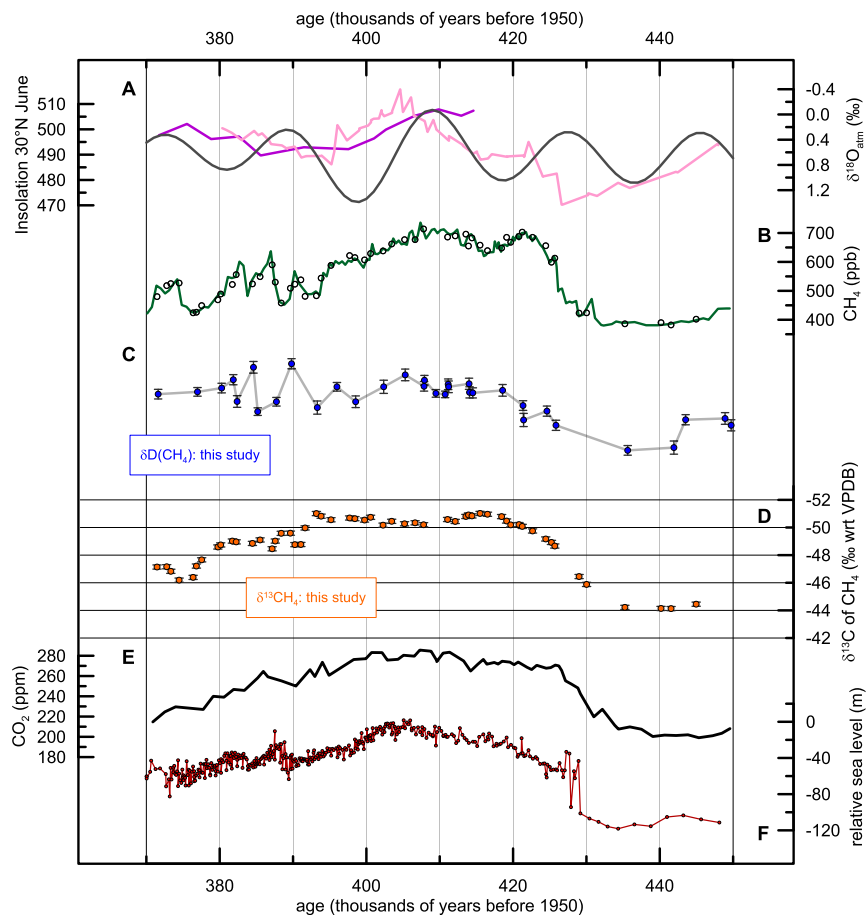


Fig. S5. Paleoclimatic records of Fig. 1 zoomed for MIS 12 and MIS 11.3. From top to bottom, the panels show (A) solar insolation in June at 30° N (133) and atmospheric $\delta^{18}\text{O}$ from Vostok (purple) (134), and EDC (light pink) (51, 135); (B) $[\text{CH}_4]$ (ref. 4 and data from this study); (C) $\delta\text{D}(\text{CH}_4)$ from EDML and EDC (this study; error bars are 1-sigma SDs of reference air measurements); (D) $\delta^{13}\text{CH}_4$ from Talos Dome, EDC, and Vostok (5G; this study; the error bars represent the 1-sigma SD of ice core replicates (47): 0.15‰) and data from EDML and Vostok (25, 32); (E) $[\text{CO}_2]$ (110); and (F) relative sea level as reconstructed from Red Sea sediment cores (108).

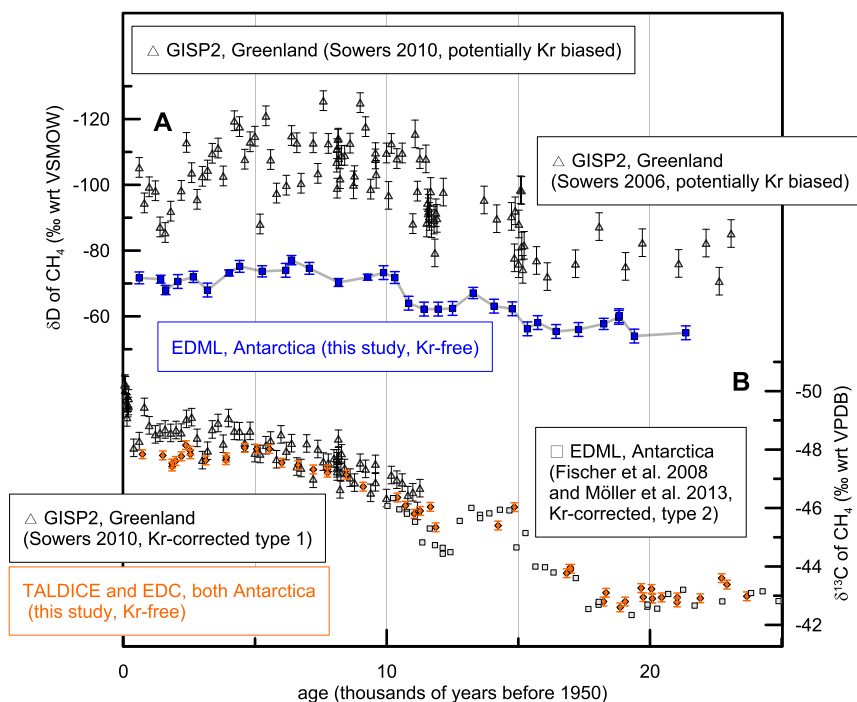


Fig. 56. Comparison of previously published datasets with this study for the last 25,000 y. (A) $\delta D(CH_4)$ by Sowers (31, 49) from the Greenland core Greenland Ice Sheet Project (GISP2) and data from this study from EDML (Antarctica). Note that the offset of the two datasets is caused by a not well-quantified IPD in $\delta D(CH_4)$ (approximately -16%) plus an interlaboratory-scale offset (46). Additional slight differences might occur, because the datasets by Sowers (31, 49) are not free from a Kr effect, whereas $\delta D(CH_4)$ data from this study are measured without any Kr interference (46). (B) $\delta^{13}C$ from the Greenland core GISP2 (49), data from EDML (32), and data from this study from TALDICE and EDC (all three cores from Antarctica). Also for $\delta^{13}C$, the IPD is not well-known (approximately -0.5%). We stress that only the $\delta^{13}C$ data of this study are measured without any Kr interference (47, 48). The data by Sowers et al. (49) and Fischer et al. (32) have been corrected for a Kr effect by ref. 25 using two different approaches: the correction ($\Delta\delta^{13}C_{Kr}$) of Vostok and GISP2 data measured at the Pennsylvania State University were inferred indirectly from CH_4 mixing ratios (referred to as type 1), whereas for the EDML record, the correction was based on the Kr-induced anomaly derived from the ion current ratios (type 2; section 1.3 of ref. 25 has a detailed description of both approaches).

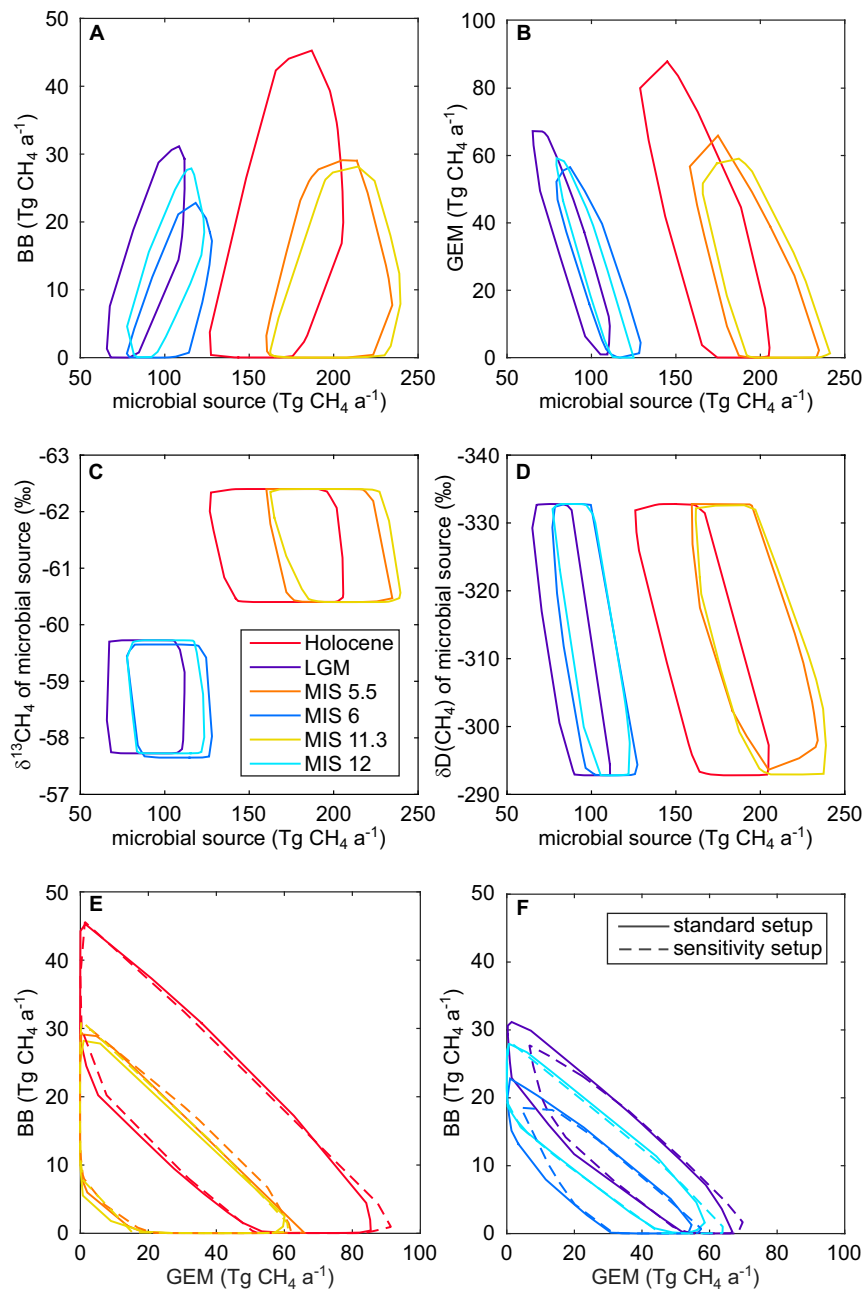


Fig. S7. Box model results fulfilling the ice core constraints. Each line encloses 10,000 valid realizations of the Monte Carlo model covering the parameter spaces of six time periods (Table S1). The Matlab function `convhull()` was used to determine the envelope around the solutions for each time slice. Legends are valid for all subpanels. (A and B) Shown are emission strengths of the microbial model source in relation to (A) BB and (B) GEM for interglacial and glacial times. (C and D) Shown are emission strengths of the microbial model source in relation to its isotopic signature: (C) $\delta^{13}\text{CH}_4$ and (D) $\delta\text{D}(\text{CH}_4)$ for interglacial and glacial times. $\delta^{13}\text{CH}_4$ of the microbial source is chosen to be heavier by 2.6‰ for glacial (in the text and Table S2). (E and F) Box model results of the standard setup (lines) and the sensitivity runs with zero IPD of $[\text{CH}_4]$ (dashed lines). Shown are emission strengths of BB in relation to GEM. E shows results for interglacials, and F shows results for glacial.

Table S1. Quantitative estimates of the mean methane stable isotopic signature (this study) and mixing ratios (4) characterizing the time slices used in the box model

Minimum gas age AICC (ka BP)	Maximum gas age AICC (ka BP)	Used ice core(s)	N	Mean	SD	Median	Minimum	Maximum	Corresponding MIS
$\delta^{13}\text{CH}_4$ (‰ wrt VPDB)									
0.5	11.6	TALDICE and EDC	26	-47.4	0.7	-47.6	-48.2	-45.8	MIS 1
17.3	24.6	TALDICE	15	-43.0	0.3	-42.9	-43.6	-42.6	MIS 2
120.1	129.7	TALDICE, EDC, Vostok	16	-50.1	0.7	-50.4	-51.0	-48.7	MIS 5.5
136.6	146.1	TALDICE and EDC	5	-45.5	0.2	-45.5	-45.8	-45.3	MIS 6
394.0	426.6	EDC	26	-50.3	0.6	-50.5	-51.0	-48.7	MIS 11.3
434.0	447.2	EDC	4	-44.2	0.1	-44.2	-44.4	-44.1	MIS 12
$\delta\text{D}(\text{CH}_4)$ (‰ wrt VSMOW)									
0.5	11.6	EDML	18	-71	4	-72	-77	-62	MIS 1
17.3	24.6	EDML	5	-57	3	-58	-60	-54	MIS 2
120.1	129.7	EDML and EDC	14	-92	4	-92	-100	-86	MIS 5.5
136.6	146.1	EDC	3	-66	4	-68	-70	-61	MIS 6
394.0	426.6	EDC	18	-88	5	-89	-96	-76	MIS 11.3
434.0	447.2	EDC	3	-71	7	-67	-78	-66	MIS 12
[CH ₄] (ppb)									
0.5	11.6	EDC	280	618	40	612	549	717	MIS 1
17.3	24.6	EDC	44	377	15	375	351	409	MIS 2
120.1	129.7	EDC	47	634	45	627	535	726	MIS 5.5
136.6	146.1	EDC	17	382	24	375	342	432	MIS 6
394.0	426.6	EDC	87	649	47	658	498	736	MIS 11.3
434.0	447.2	EDC	9	391	8	392	381	405	MIS 12

Note the large SDs, especially for $\delta^{13}\text{CH}_4$ and [CH₄] during interglacials, indicative of the large signal ranges observed within these time periods (compare Fig. 1 and Figs. S2–S5). Red and blue colors represent interglacial and glacial time slices, respectively, in line with colored bars in Fig. S1. Columns from left to right give the minimal and maximal gas ages of the analyzed time periods on the Antarctic ice core chronology (AICC 2012) age scale; the names of the ice cores used; the number of samples (N), average (mean), SD, median, minimum value, and maximum value for [CH₄], $\delta^{13}\text{CH}_4$, $\delta\text{D}(\text{CH}_4)$; and the MIS roughly corresponding to the ice core time slices.

Table S2. Ranges of isotopic source signatures and source strengths used as model input

Source category	$\delta^{13}\text{C}-\text{CH}_4$ minimum (‰ wrt VPDB)	$\delta^{13}\text{C}-\text{CH}_4$ maximum (‰ wrt VPDB)	$\delta\text{D}-\text{CH}_4$ minimum (‰ wrt VSMOW)	$\delta\text{D}-\text{CH}_4$ maximum (‰ wrt VSMOW)	Global source strength minimum (Tg CH ₄ a ⁻¹)	Global source strength maximum (Tg CH ₄ a ⁻¹)
Standard model setup						
Interglacials						
Microbial source (south)	-62.4	-60.4	-332.8	-292.8	50	250
Microbial source (north)	-63.6	-61.6	-343.1	-303.1	0	60
BB	-24.7	-20.0	-255.0	-195.0	0	120
GEM	-44.9	-43.2	-205.0	-165.0	0	
Glacials						
Microbial source (south)	-59.7	-57.7	-332.8	-292.8	20	150
Microbial source (north)	-60.9	-58.9	-343.1	-303.1	0	60
BB	-22.0	-17.3	-255.0	-195.0	0	120
GEM	-44.9	-43.2	-205.0	-165.0	0	
Adjusted microbial source for sensitivity runs (assuming no IPD of [CH ₄])						
Interglacials						
Microbial source (south)	-62.3	-60.3	-332.8	-292.8	50	250
Microbial source (north)	-64.0	-62.0	-347.3	-307.3	0	60
Glacials						
Microbial source (south)	-59.6	-57.6	-332.8	-292.8	20	150
Microbial source (north)	-61.3	-59.3	-347.3	-307.3	0	60

For every Monte Carlo model run, values for $\delta^{13}\text{CH}_4$, $\delta\text{D}(\text{CH}_4)$, and the source strengths of each of three model source categories have been randomly picked from the given intervals. wrt, with respect to. The Matlab function unifrnd() has been used to generate continuous uniform random numbers. References and adjustments for the given isotopic signatures are described in detail in *SI Text* (refs. 13, 22, 32, 36, and 63 and references therein). Note that, concerning the microbial source, different isotopic signatures for the Southern Hemisphere and Northern Hemisphere are used. All source strengths are given as global values and distributed between the hemispheres according to information given in the text. Note the changed isotopic signatures for the microbial source for the sensitivity runs that assume no IPD of CH₄.

Table S3. Model sink fractions, isotopic fractionation factors, and hemispheric distribution

Sink	Sink fraction minimum (%)	Sink fraction maximum (%)	Fractionation factor ϵ for $\delta^{13}\text{CH}_4$ (‰)	Fractionation factor ϵ for $\delta\text{D}(\text{CH}_4)$ (‰)	Northern Hemisphere fraction of sink (%)
Tropospheric OH	78.8	84.8	-5.4	-231	50
Stratospheric loss	7.6	11.0	-22	-80	50
Soils	3.9	5.6	-12	-160	73.8
Tropospheric Cl	3.4	5.0	-60	-470	43.1

For every Monte Carlo model run, sink fractions of the individual sink processes have been randomly picked from the given intervals to account for uncertainties in the sink apportionment. Fractionation factors and hemispheric distribution have been kept constant for all model runs.